Materials Research. 2016; 19(6): 1335-1343
DOI: http://dx.doi.org/10.1590/1980-5373-MR-2015-0660

Comprehensive Study of Growth Mechanism and Properties of Low Zn Content $Cd_{1-x}Zn_xS$ Thin Films by Chemical Bath

Carlos Aníbal Rodríguez [a]*, Myrna Guadalupe Sandoval-Paz [b], Renato Saavedra[b,c], Cuauhtémoc Trejo-Cruz [d], Francisco De la Carrera [b], Luis E. Aragon[e], Martín Sirena [e], Marie-Paule Delplancke[f], Claudia Carrasco [g]

[a] *Multidisciplinary Research Institute in Science and Technology, Ineergias, University of La Serena, Benavente 980, La Serena, Chile*
[b] *Department of Physics, Faculty of Physical and Mathematical Sciences, University of Concepción, Esteban Iturra s/n, Casilla 160-C, Concepción, Chile*
[c] *Center for Optics and Photonics, Universidad de Concepción, Casilla 4016, Concepción, Chile*
[d] *Department of Physics, Faculty of Sciences, University of Bíobio, Avenida Collao 1202 casilla 5C, Concepción 4051381, Chile*
[e] *Centro Atómico Bariloche & Instituto Balseiro, CNEA & Univ. Nac. de Cuyo, Av. Bustillo 9500, 8400 Bariloche, Rio Negro, Argentina*
[f] *4MAT, Université Libre de Bruxelles, Avenue Roosevelt 50, CP 165/63, Brussels 1050, Belgium*
[g] *Department of Materials Engineering, Faculty of Engineering, University of Concepción, Edmundo Larenas 270, Concepción 4070409, Chile*

Received: October 30, 2015; Revised: August 18, 2016; Accepted: September 04, 2016

$Cd_{1-x}Zn_xS$ thin films have been studied extensively as window layers for solar cell applications. However, a mismatch between the $Cd_{1-x}Zn_xS$ and copper–indium–gallium–selenide absorber layers increases with Zn film concentration, which reduces the device efficiency. In this work, $Cd_{1-x}Zn_xS$ thin films with low Zn concentrations were analyzed. The effect of the addition of different molar Zn concentrations to the reaction mixture on the growth mechanism of $Cd_{1-x}Zn_xS$ thin films and the influence of these mechanisms on structural, optical and morphological properties of the films has been studied. $Cd_{1-x}Zn_xS$ thin films were synthesized by chemical bath deposition using an ammonia-free alkaline solution. Microstructural analysis by X-ray diffraction showed that all deposited films grew with hexagonal structure and crystallite sizes decreased as the Zn concentration in the film increased. Optical measurements indicated a high optical transmission between 75% and 90% for wavelengths above the absorption edge. Band gap value increased from 2.48 eV to 2.62 eV, and the refractive index values for $Cd_{1-x}Zn_xS$ thin films decreased as the Zn increased. These changes in films and properties are related to a modification in growth mechanism of the $Cd_{1-x}Zn_xS$ thin films, with the influence of $Zn(OH)_2$ formation being more important as Zn in solution increases.

Keywords: *$Cd_{1-x}Zn_xS$; chemical bath deposition; optical properties; structural properties.*

1. Introduction

$Cd_{1-x}Zn_xS$ thin films have attracted attention for a long time, since their energy band gap can be tuned and their lattice parameters can be modified with variation in Zn concentration[1-3]. Replacement of CdS with higher energy gap ternary $Cd_{1-x}Zn_xS$ in thin-film solar cells, based on CdTe or copper–indium–gallium–selenide (CIGS) absorbers, is expected to decrease window absorption losses and result in an improved solar cell performance[4,5]. Several studies have focused on the deposition of $Cd_{1-x}Zn_xS$ thin films with different Zn contents[6-8], but the Zn content that has been studied thus far has always been larger than 5 at.%. Therefore, the range of very low Zn contents below 5% has not been studied to date. An investigation of this small range of compositions increased in importance because, as reported by Burton et al.[9] and Reddy et al.[10], a higher Zn concentration leads to a large lattice mismatch with CIGS-absorber material and a higher resistivity material, which increases the series resistance of thin-film solar cell devices. The lattice mismatch between window and absorbent layers is important to considerer in heterojunction solar cell device manufacture. Defects in junctions introduce energy levels in the band structure, which act as recombination sites and reduce the conversion efficiency of the devices[11]. A near-perfect lattice match is obtained between the absorber CIGS-(1 1 2) tetragonal plane and the window CdS-(1 0 0) hexagonal phase plane. Accordingly, the Zn concentration in $Cd_{1-x}Zn_xS$ films should be kept as low as possible, whereas

* e-mail: arodriguez@userena.cl

the optical transmission and band gap should be increased as much as possible.

$Cd_{1-x}Zn_xS$ thin films were deposited by chemical bath deposition (CBD), which is a very simple, inexpensive and effective technique for the deposition of various semiconductor materials. It is well known that the initial reaction solution conditions in CBD determine the properties of the obtained films; however, few studies have focused on the growth mechanisms and subsequent film properties. Hodes et al.[3] concluded that the thickness and crystal size of thin films produced by CBD are strongly dependent on growth mechanisms. Therefore, it is also possible to relate the optical film properties to the growth mechanism. For example, Rodríguez et al. demonstrated that the growth mechanism affects the morphological properties and chemical composition of ZnS thin films grown by CBD from a non-toxic alkaline solution[12], which can affect optical properties.

Another important factor in the synthesis of $Cd_{1-x}Zn_xS$ thin films by CBD is the reaction solution composition. Most reports found in literature use ammonia as complexing agent in the aqueous synthesis of semiconductor thin films[1,2,6,7]. However, this is a highly volatile, toxic and harmful material[8], and industrial production would produce serious environmental and health problems. Considering the large amount of waste derived from the deposition process, the use of non-toxic precursors in film synthesis reduces the current environmental crisis.

We present on a detailed study of the growth mechanisms involved in CBD of the $Cd_{1-x}Zn_xS$ ternary compound to understand the synthesis of $Cd_{1-x}Zn_xS$ thin films better. The effects of very low Zn concentration (less than 5 at.%) on chemical, structural, optical and morphological properties are analyzed and interpreted in terms of growth mechanisms.

2. Experimental Procedure

$Cd_{1-x}Zn_xS$ thin films with low Zn content were deposited on glass slide substrates using an ammonia-free CBD process, which has been used previously to deposit CdS thin films[13,14] and aqueous solutions of 0.05 M $CdCl_2$, 0.5 M $C_6H_5O_7Na_3$ (sodium citrate, Sigma-Aldrich), 0.5 M KOH (J.T. Baker), pH 10 borate buffer solution (Winkler), and 0.5 M $CS(NH_2)_2$ (thiourea, Sigma-Aldrich). Five types of $Cd_{1-x}Zn_xS$ films were studied, where the Zn concentration in the reaction mixture was increased from 0 (used as reference) to 1.5×10^{-3} M by adding $Zn(CH_3COO)_2$ (Sigma-Aldrich), while maintaining all other reactant concentrations unchanged. The molar ratio, r = [Zn]/[Zn+Cd], in each reaction solution was 0, 0.05, 0.07, 0.09, and 0.13. All studied thin films were deposited at a solution temperature of 70°C and pH 11.5. Four samples were deposited for each condition by placing four substrates in the reaction beaker and then removing them from solution after 15, 30, 60, and 90 min, respectively. The films obtained were yellowish, homogeneous, specularly reflecting, and adhered well to the glass substrate.

To study the mechanisms of growth, a speciation diagram was produced according to the procedure reported by Tec-Yam et al.[15].

The film chemical composition was obtained by total reflection X-ray fluorescence (TXRF) using a Bruker S2 PICOFOX spectrometer. Structural analysis was by X-ray diffraction (XRD) using a D4 ENDEAVOR diffractometer with Cu Kα radiation. The optical transmittance spectra were measured with an optical fibre spectrometer (Ocean Optics USB 4000). The sample surface morphology was studied by atomic force microscopy (AFM) using a NANOSCOPE IIIa in contact mode.

3. Results and Discussion

$Cd_{1-x}Zn_xS$ thin-film growth can be understood from the reactions occurring in solution. In a cadmium–citrate–thiourea reaction system under alkaline conditions, the citrate ion (Cit^{3-}) acts as a complexing agent, which controls the Cd^{2+} ion concentration through the reaction reported by Treumann et al.[16]:

$$CdCl_2 \longrightarrow Cd_2 ++ 2Cl^- \quad (1)$$

$$Cd^{2+} + Cit^{3-} \longleftrightarrow CdCit^-, k_s = 2.3\times10^5 \quad (2)$$

where k_s is the stability constant of the $CdCit^-$ complex ion.

Sulfur ions, S^{2-}, are released from thiourea and react with Cd^{2+} ions:

$$SC(NH_2)_2 + OH^- \longrightarrow SH^- + CH_2N_2 + H_2O \quad (3)$$

$$SH^- + OH^- \longrightarrow S^{2-} + H_2O \quad (4)$$

$$Cd^{2+} + S^{2-} \longrightarrow CdS_{(s)} \quad (5)$$

Eq. (5) is the chemical bath growth mechanism termed 'ion by ion mechanism'.

In the same way, free Cd^{2+} ions can react with OH^- ions contained in solution to form insoluble cadmium hydroxide:

$$Cd^{2+}{}_{(aq)} + 2OH^-{}_{(aq)} \longrightarrow Cd(OH)_{2,(s)} \quad (6)$$

This metal hydroxide reacts with S^{2-} ions released from thiourea decomposition to form CdS according to:

$$Cd(OH)_{2,(aq)} + S^{2-}{}_{(aq)} \longrightarrow CdS_{(S)} + 2OH^-{}_{(aq)} \quad (7)$$

Reaction (7) occurs because k_{sp} for CdS (10^{-28}) is much smaller than the corresponding value for $Cd(OH)_2$ (2×10^{-14})[3], i.e., the free energy change required for reaction (7) is more negative, and the reaction occurs spontaneously.

When Zn^{2+} is added to the solution, it is also complexed by citrate ions through the following reaction reported by Martin et al.[17]:

$$Zn(CH_3COO)_2 \longrightarrow Zn^{2+} + 2(CH_3COO)_2 \quad (8)$$

$$Zn^{2+} + Cit^{3-} \longleftrightarrow ZnCit^{-}, k_s = 6.31 \times 10^4 \quad (9)$$

On the other side, free Zn^{2+} ions react with OH^- ions, to form zinc hydroxide:

$$Zn^{2+}{}_{(aq)} + 2OH^-{}_{(aq)} \longrightarrow Zn(OH)_{2,(s)} \quad (10)$$

which can react with S^{2-} ions to form ZnS:

$$Zn(OH)_{2,(aq)} + S^{2-}{}_{(aq)} \longrightarrow ZnS_{(s)} + 2OH^-{}_{(aq)} \quad (11)$$

Reaction (11) occurs because k_{sp} for ZnS (10^{-25}) is much smaller than the k_{sp} for $Zn(OH)_2$ (10^{-16}) and, from $\ln(k_{sp}) = \Delta G^0/RT$, ZnS has a lower free energy change than $Zn(OH)_2$. According to Hodes [3], since CdS and ZnS have different solubility product constants, the formation of a ternary compound would occur by precipitation of CdS, which adsorbs S^{2-} and Zn^{2+} ions to form a ZnS layer. This eventually diffuses to form a solid solution of $Cd_{1-x}Zn_xS$. Figure 1 shows a schematic representation of $Cd_{1-x}Zn_xS$ ternary compound precipitation. Side (A) corresponds to a process described above and side (B) corresponds to a process involving any hydroxide mechanism. According to reactions (6) and (10), Cd^{2+} and Zn^{2+} can react with OH^- ions to form metallic hydroxides. As the reaction proceeds, these metallic hydroxides transform to sulfides as expressed by reactions (7) and (11). A diagram of species distribution was conducted to obtain a better understanding of the formation of $Cd_{1-x}Zn_xS$ through metallic hydroxide intermediates species. Groups of intermediate chemical species formed during chemical reaction can be obtained from this diagram, bearing in mind that the dominant species depend strongly on chemical reagents used in the chemical bath.

In the reaction solution, Zn^{2+} and Cd^{2+} ions can react with dissolved OH^- and Cit^{3-} ions to form several soluble species, but our study is interested specifically in $Zn(OH)_2$ and $Cd(OH)_2$ species. Table 1 shows the chemical reactions and their corresponding formation (β) and dissociation (*K*) constants at 25°C reported in literature. In all cases, the equilibrium constants were calculated by considering the concentration (mol×L^{-1}), knowing that $[OH^-][H^+]=10^{-14}$ mol×L^{-2}, and taking Cd^{2+} as reference. Figure 2 shows the repartition of species, s_i, as a function of pH. For a pH between 8.5 and 10.5, $Zn(OH)_2$ is the predominant species. Above pH 10.5, the predominant species is $Cd(OH)_2$. Thus, at a pH of 11.5, $Cd_{1-x}Zn_xS$ ternary compound formation proceeds via $Cd(OH)_2$. This process is shown in Figure 1, side (B), where it can be seen that $Cd(OH)_2$ would adsorb S^{2-} and Zn^{2+} ions to form a ternary compound. It should also be noted that, because of the lower k_{sp} for $Zn(OH)_2$ than for $Cd(OH)_2$, growth may result through $Zn(OH)_2$ species affecting film properties as r increases.

$Cd_{1-x}Zn_xS$ film composition was determined by TXRF analysis (see Table 2). The film content (x) does not match that of the solution ratio r. Similar results have been reported previously[8,21]. Considering the high pH values, it is expected that Zn^{2+} ions react with OH^- ions to precipitate $Zn(OH)_2$ to a large extent, in the solution bulk. Therefore, a deficit in Zn content, x, could be expected from the amount of Zn that does not participate in the film growth process as a result of $Zn(OH)_2$ formation. This idea, and the influence of $Zn(OH)_2$ phase on thin-film properties, will be discussed further and developed.

Figure 3 shows XRD patterns of the $Cd_{1-x}Zn_xS$ thin films obtained after 90 min reaction time. The pattern obtained from a CdS film (r = 0) shows an intense peak centred at 26.7°, which corresponds to the hexagonal phase, (002) plane (PDF#77-2306). Three less intense peaks are visible at 44°, 48° and 55°, which are produced by the hexagonal phase, (110), (103) and (004) planes, respectively. As the r ratio in solution increases from 0 to 0.13, the intensity of the (002) peak decreases and that of the (100) and (110) peaks increases.

All diffraction peaks in the patterns of the $Cd_{1-x}Zn_xS$ films are shifted towards higher angles with respect to those corresponding to hexagonal CdS, which indicates a decrease in lattice parameter, i.e., the presence of uniform strain because of the smaller ionic radii of Zn^{2+} (0.074 nm), which substitutes Cd^{2+}(0.095 nm) ions. Increasing Zn contents results in the shrinkage of the crystalline plane spacing as a consequence of the stress produced by the introduction of Zn^{2+} to the lattice [22]. In Table 3, a comparison of calculated interplanar spacing *d*-values with those of PDF#77-2306 (CdS) and PDF#40-0835 ($Cd_{0.805}Zn_{0.195}S$) are shown. It has been observed that higher doped samples result in a phase change transition from hexagonal structure to cubic form, as a consequence of substitution of Cd^{2+} by Zn^{2+} [22].To obtain more information about the ternary alloy structure, further analysis was carried out using Vegard's law. Vegard's law is an empirical rule that states that an alloy property value can be determined from a linear interpolation of the property values of its constituent elements. According to Vegard's law[22,23], lattice constants *a* and *c* of the $Cd_{1-x}Zn_xS$ alloy decrease linearly, whereas x increases from 0 to 1:

$$a = 4.136 - 0.325x$$
$$c = 6.713 - 0.479x \quad (12)$$

Parameters *a* and *c* are related to the interplanar spacing *d*, as follows [24]:

$$d_{hkl} = \frac{a}{\sqrt{\left(\frac{4}{3}\right)(h^2 + hk + k^2) + (a/c)^2 l^2}} \quad (13)$$

So, the *d*-spacing also shows a linear dependence on x. Figure 4 shows the variation in lattice constants *a* and *c*. A gradual decrease in lattice constants is observed as x increases. This trend is consistent with Vegard's law and indicates a homogeneous alloy structure[25]. From Figure 4, a negative deviation from the Vegard's law occurs, which may result from

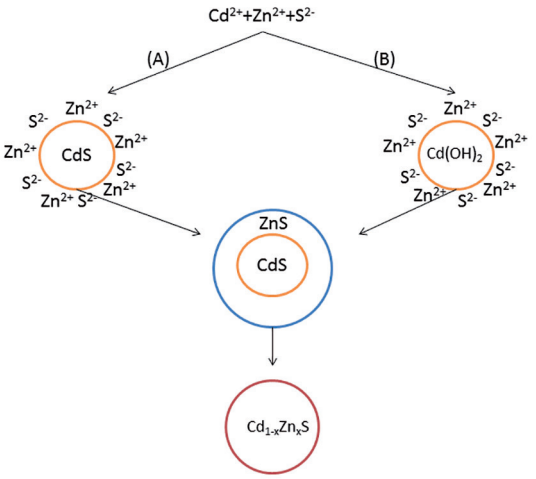

Figure 1: Scheme of possibilities for coprecipitation of $Cd_{1-x}Zn_xS$ thin films.

Table 1: Chemical reaction and their corresponding formation and dissociation constants calculated at 25°C.

Chemical reaction	Formation or dissociation constant	References
$Cd^{2+}+2OH^- \longrightarrow Zn(OH)_2$	$\beta = 10^{7.65}$	[18]
$Cd^{2+}+Cit^{3-} \longrightarrow Cd(Cit)^-$	$\beta = 10^{3.7}$	[19]
$Zn^{2+}+2OH^- \longrightarrow Zn(OH)_2$	$\beta = 10^{10.08}$	[14]
$Zn^{2+}+Cit^{3} \longrightarrow Zn(Cit)^-$	$\beta = 10^{4.98}$	[20]
$HCit^{2-} \rightarrow Cit^{3-}+H^+$	$K = 10^{-5.69}$	[20]

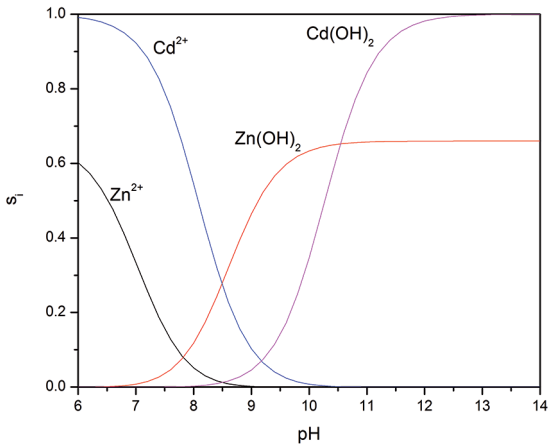

Figure 2: Distribution diagram of species for chemical bath solution from Cd–Zn–H_2O.

several factors, including: (i) the relative size of constituent elements, (ii) the relative volume per valence electron and (iii) electrochemical differences between the elements[26]. It has been suggested in literature that deviations from Vegard's law can be represented by a quadratic expression[26,27]; however, applicability of such quadratic expression to any ternary alloys is unknown. Physically, deviations from Vegard's law have been interpreted as a certain lattice disorder (related to

Table 2: TXRF analysis of $Cd_{1-x}Zn_xS$ thin films grown over 120 min.

r (Solution)	Element (at.%)			x (Film)	[S]/ [Zn+Cd]	E_g (eV)
	Cd	Zn	S			
0	56.35	0	43.65	0	0.774	2.48
0.05	56.76	1.85	41.39	0.032	0.706	2.52
0.07	52.84	3.45	43.71	0.061	0.775	2.58
0.09	61.94	2.66	35.39	0.041	0.548	2.60
0.13	55.41	4.77	39.82	0.079	0.662	2.62

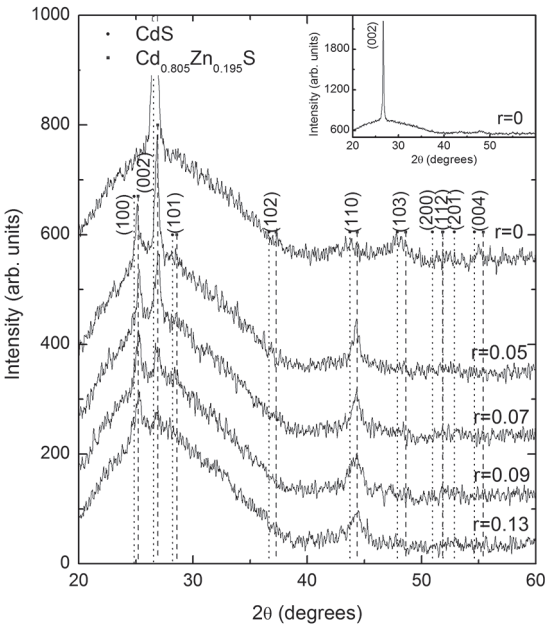

Figure 3: XRD patterns of $Cd_{1-x}Zn_xS$ films grown over 90 min.

atom position) that produce a unit cell with volume either greater or smaller than that predicted from Vegard's law[27].

Another important parameter that can be calculated from XRD patterns is the crystallite size. In many cases, the crystallite size is calculated using Scherrer's formula[24]; however, such a formula considers that there is no lattice strain, and therefore peak broadening results only from the crystallite size effects. When lattice strains are expected to appear within the sample, the Williamson–Hall (W–H) plot allows for the separation of peak broadening when both microstructural causes – i.e., small crystallite size and microstrain – occur simultaneously[28]. Figure 5a shows the W–H plot for samples with different Zn content (Zn = 0 is not considered). Bcosθ is a linear function of sinθ, which indicates that the lattice strain contributed significantly to peak broadening[24]. It can be seen from the slope of the linear fit of experimental values that there is neither change nor trend for lattice strain, as the amount of Zn increases. This suggests that, for each sample, the lattice strains contribute to peak broadening and, as the amount of Zn increases, a change (diminution) in crystallite size results that contributes

Table 3: Interplanar spacing dhkl of Cd1–xZnxS thin films.

hkl	PDF#	PDF#	r ratio in reaction solution				
	77-2306	40-0835	0	0.05	0.07	0.09	0.13
	CdS	$Cd_{0.805}Zn_{0.195}S$					
100	3.5819	3.5300	-	3.5446	3.5206	3.5276	3.5186
002	3.3565	3.3100	3.3370	3.3193	3.3087	3.3133	3.3179
101	3.1602	3.1200	-	-	-	-	-
102	2.4492	2.4100	-	-	-	-	-
110	2.0680	2.0400	-	2.0448	2.0435	2.0406	2.0364
...							

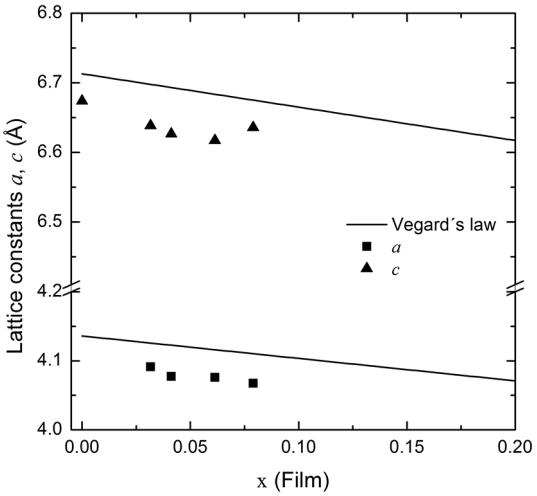

Figure 4: Crystal lattice constants as a function of Zn film content (x).

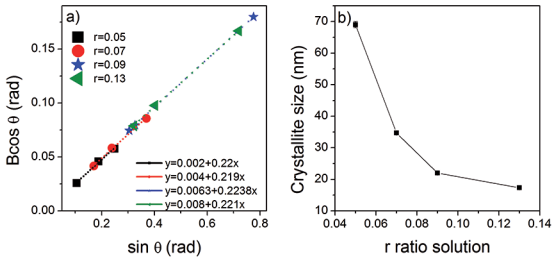

Figure 5: a) Williamson–Hall plot and b) crystallite size as a function of solution r ratio.

to peak broadening. The crystallite size calculated from the Y-intercept of the W–H plot is shown in Figure 5b as a function of r ratio in reaction solution. As r increases in solution, there is a clear decrease in crystallite size. This result could be a consequence of growth mechanism, which is favored by deposition conditions: a large concentration of OH^- ions exists at pH 11.5; when Zn^{2+} is added to solution, $Zn(OH)_2$ forms according to reaction (10). When $Zn(OH)_2$ protrudes from the solution to the substrate, the crystal size is not expected to change much with film thickness because the ionic exchange between OH^- and S^{2-} occurs instead of another growth process. This could explain why the obtained crystallite size decreases as the Zn concentration increases.

The thickness and optical properties of $Cd_{1-x}Zn_xS$ films were obtained by analysing the corresponding optical transmittance spectra. In Figure 6, the transmittance spectra of $Cd_{1-x}Zn_xS$ thin films deposited at different deposition times are shown. The absorption edge is at a.c. 500–520 nm in CdS films (x = 0), which agrees well with values reported in literature[2,25]. As the Zn concentration increases in the $Cd_{1-x}Zn_xS$ films, the absorption edge shifts to shorter wavelengths for all deposition times. The transmittance is between 75 and 90% at wavelengths longer than the absorption edge, which indicates that most incident light will be transmitted throughout the material. To estimate the film thickness and optical constants *n* and *k*, respectively, the transmittance spectra were fitted to a layer model by considering the samples as constituted by an air/roughness/$Cd_{1-x}Zn_xS$/glass system as reported in refs[13,14]. The $Cd_{1-x}Zn_xS$ optical constants were represented by the SCI® model, which is a generalized version of the Lorentz harmonic oscillator expression, consistent with the Kramers–Kronig relationships[29]. The model defines a complex dielectric function $\varepsilon = \varepsilon_1 + i\varepsilon_2$, wherein ε_1 and ε_2 are the real and imaginary part of the dielectric function, and is defined as follows:

$$\varepsilon_1^* = \sum_{j=1}^{m} \frac{A_j^2\left(E^2 - (E_{center})_j^2\right)}{\left[E^2 - (E_{center})_j^2\right] + v^2E^2} \quad (14)$$

$$\varepsilon_2^* = \sum_{j=1}^{m} \frac{A_j^2 Ev}{\left[E^2 - (E_{center})_j^2\right] + v^2E^2} \quad (15)$$

if $\varepsilon_2^* > \varepsilon_1^*$ or $E > E_{center}$, then

$$\varepsilon_1 = \varepsilon_\infty(\varepsilon_1^* - \varepsilon_2^*\alpha E + 1) \quad (16)$$

$$\varepsilon_1 = \varepsilon_\infty(\varepsilon_2^* - \varepsilon_1^*\alpha E) \quad (17)$$

Else

$$\varepsilon_1 = \varepsilon_\infty(\varepsilon_1^* - \varepsilon_2^*\alpha E + 1) \quad (18)$$

$$\varepsilon_2 = 0$$

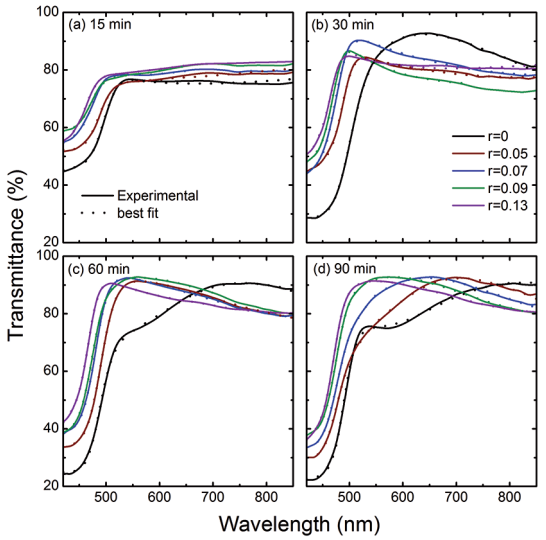

Figure 6: Optical transmittance spectra of $Cd_{1-x}Zn_xS$ deposited at different deposition times, and different r ratios in reaction solution.

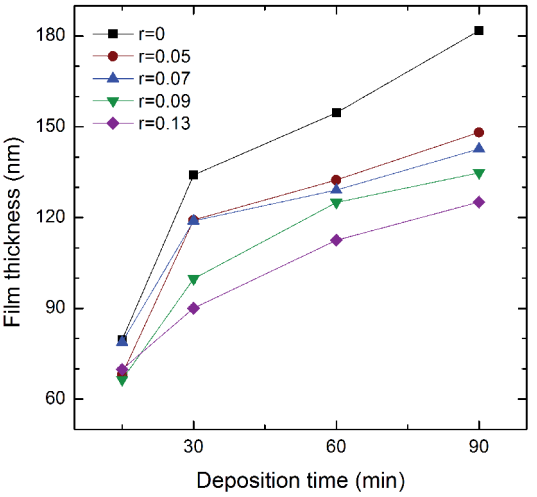

Figure 7: Film thickness as a function of deposition time and r ratio in reaction solution.

Where ε_∞ is the high-frequency lattice dielectric constant, $(E_{center})_j$ is the center energy of each oscillator which is related to the transverse phonon frequency. A_j is the amplitude (strength) of each oscillator and it is related to both the transverse and longitudinal phonon frequencies. v_j is the vibration frequency (broadening) of the "j" oscillator. E is the energy and α is the damping coeficient. In the limit of α=0 the dispersión formula reduces to the Lorentz oscillator model. In the adjustment process are allowed to vary all parameters of the model to find the best optimization given by values of root mean squared error (RMSE) less than 1. The model estimation of roughness was given by the thickness of this layer. In Figure 6, the dotted lines represent best fits to the proposal layers model. Good agreement exists between experimental data and the theoretical fit. From the fitting procedure, the thickness, roughness and optical constants *n* and *k* for all the films were obtained. The roughness values ranged between 3 and 6 nm for all samples, and showed no clear trend with Zn film concentration.

In Figure 7, the film thickness is shown as a function of deposition time for all $Cd_{1-x}Zn_xS$ thin films. In the early stages of deposition, up to 30 min, all $Cd_{1-x}Zn_xS$ films exhibit a higher growth rate, which decreases as the r ratio in solution increases. After 30 min, the growth rate decreases in all cases. This occurs because of a decrease in reactant concentration as the reaction proceeds. Two interesting facts are that (i) the growth rate is slower as the Zn concentration in solution increases, (ii) the film thickness decreases as the Zn concentration increases. These two facts are related, and can be explained by considering the participation of a hydroxide growth mechanism. The decreasing thickness and growth rate are expected from the previously suggested hydroxide growth mechanism. Since initial hydroxide nucleation occurs homogeneously in solution, the compound is also formed homogeneously and therefore usually precipitates out in solution to a large extent. Thus, as the Zn concentration increases, this effect is expected to increase, which results in a slower film growth rate and therefore thinner films. The film thickness after 90 min deposition was a.c. 180 ± 0.7, 150 ± 0.3, 143 ± 0.3, 135 ± 0.2, and 125 ± 0.1 nm, for r = 0, 0.05, 0.07, 0.09, and 0.13, respectively.

The optical constants *n* and *k* as a function of the wavelength obtained from the fitted transmittance spectra are shown in Figure 8 for thin films deposited during 90 min. As expected, the *n* spectra shape is similar to that obtained from analysis of an ellipsometric spectrum of CdS films reported previously in literature[13,14]. The maximum in the *n* spectrum at ~480 nm (2.58 eV) for CdS films (x = 0) is related to optical transitions at a fundamental absorption edge of the CdS wurzite crystalline lattice. The position of the maximum in the *n* spectra indicates that the absorption edge is shifted to higher energy values for $Cd_{1-x}Zn_xS$ films. This result matches a shift to higher energies of the absorption edge observed for $Cd_{1-x}Zn_xS$ films in the transmittance spectra.

The extinction coefficient spectra of the $Cd_{1-x}Zn_xS$ films also show a shift to shorter wavelengths in the absorption region, as the Zn content increases in the films. This shift is related to the increase in band gap, as x increases. To estimate the energy band gap, E_g, of the films, the model for allowed direct transitions between parabolic energy bands was used as given by[30]:

$$\alpha(\mathrm{hv}) = \mathrm{A} \times (\mathrm{hv} - \mathrm{E_g})^{1/2} \qquad (19)$$

where A^* is a constant that depends on the semiconductor, hν is the incident radiation energy, and α is the absorption coefficient. The absorption coefficient is related to the extinction coefficient *k* and wavelength by:

$$\alpha = 4\pi k/\lambda \quad (20)$$

The α^2 curve as a function of $h\nu$ can be obtained by considering the k spectra and equations (14) and (15). By extrapolating the linear portion of this curve to the x axis (where $\alpha^2 = 0$), the obtained result is $h\nu = E_g$. The calculated band gap values are shown in Table 2. An increase in band gap with Zn content is observed, as expected from the formation of the $Cd_{1-x}Zn_xS$ ternary compound. The atomic percentage of Zn in the films does not exceed 4.77% (see Table 2), while a band gap value of 2.62 eV is reached. The same band gap value is reached, as reported by Carreón et al.[8], when the atomic percentage of Zn is 7%. This observation suggests that not only the concentration of alloy dopant is influencing the band gap values. The dependence between band gap width and crystallite size has been investigated by several authors and attributed to quantum confinement effects[31,32]. The latter occurs when the crystallite size is comparable with the Bohr exciton radius, where the continuum of energy levels is broken down into discrete states with an energy level spacing > kT, which results in a widening of band gap[33]. The expected band gap resulting from quantum confinement is given by the following relation[32]:

$$E_g = E_g^{bulk} + E_b\left(\frac{2\pi a_B}{D}\right)^2 \quad (21)$$

where E_g is the measured band gap energy value, E_g^{bulk} is the expected bulk band gap energy value, E_b is the exciton binding energy, a_B is the exciton Bohr radius, and D is the average crystallite size (assumed to have a spherical shape), calculated from Scherrer's formula. Crystallite size cannot be calculated from a W–H plot, when only one diffraction peak appears (as occurs in the CdS sample). For this reason, in such a case, Scherrer's formula has been used to estimate D. By adjusting the experimental data to $E_g = A + B/D^2$, it is possible to obtain the fitting parameters $A = E_g^{bolk}$ and $B = 4E_b\pi^2a^2_B$. Figure 9 shows the relationship between band gap values and crystallite size, which has been obtained experimentally. From the fitting process, the A and B parameters were 2.51 eV and 8.18 eV·nm^2, respectively, and they agree well with theoretical values (A = 2.42 eV and B = 9.60 eV·nm^2 for hexagonal CdS at room temperature[32,34]). The discrepancy between calculated and theoretical B parameter may be attributed to several factors, such as the coulomb interaction between charge carriers, or the existence of intermediate or weak confinement[32]. The difference between calculated and theoretical A is probably because of non-stoichiometric CdS films and the formation of ternary $Cd_{1-x}Zn_xS$ compound. From these results, it can be concluded that the dependency of band gap on crystallite size may be attributed, in this work, to quantum confinement. Thus, the wide band gap exhibited by samples when compared with other work, could be related to a quantum confinement effect that results from a large reduction in crystallite size.

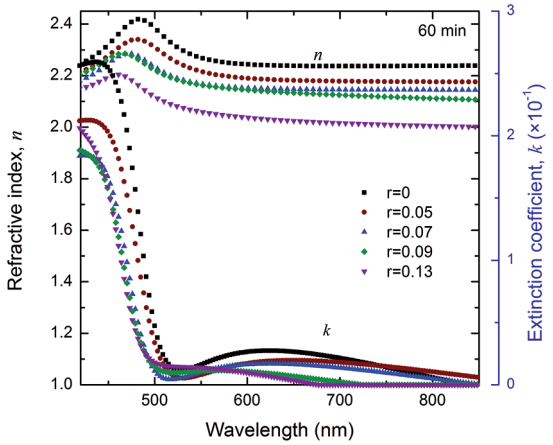

Figure 8: Refractive index (n) and extinction coefficient (k) as a function of wavelength of $Cd_{1-x}Zn_xS$ with different r ratio in reaction solution.

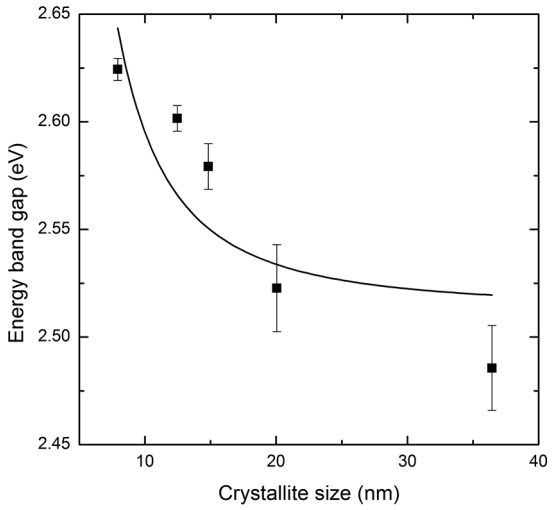

Figure 9: Energy band gap dependence of crystallite size for $Cd_{1-x}Zn_xS$ films.

Table 4 compares the most noteworthy result obtained in this work with those reported in literature. In this work, a higher E_g value was reached with lowest Zn concentration, which is a phenomenon attributed to a quantum confinement effect. The lattice mismatch between (1 0 0) hexagonal plane of $Cd_{1-x}Zn_xS$ (for the sample with 2.62 eV) and the (1 1 2) tetragonal plane of CIGS (considering $d_{(1\,1\,2)}$ = 0.366 nm) was 3.8%. This value is the lowest calculated mismatch compared with those presented in Table 4. Thus, a low Zn concentration in $Cd_{1-x}Zn_xS$ ternary compounds will result in a low lattice mismatch with absorbent CIGS layer and reduce losses in solar cell devices.

The surface morphology of $Cd_{1-x}Zn_xS$ thin films was investigated by AFM. Figure 10 shows the AFM images of $Cd_{1-x}Zn_xS$ films deposited on a glass substrate for x = 0 and 0.079, during 90 min. From the images, uniform and compact particles are observed with a clear decrease in particle

Table 4: Comparison of Zn concentration, calculated mismatch and band gap presented in this work with that reported in literature.

	Zn concentration (% at.)	Mismatch (%) with (1 1 2) plane of CIGS	Band gap (eV)
This work	4.77	3.87	2.62
S. Borse et al.[36]	25.15	5.36	2.60
Y. Raprakash et al.[37]	10.36	3.20	2.55
	20.59	4.64	2.70
U. Verma et al.[38]	14.87	4	2.63

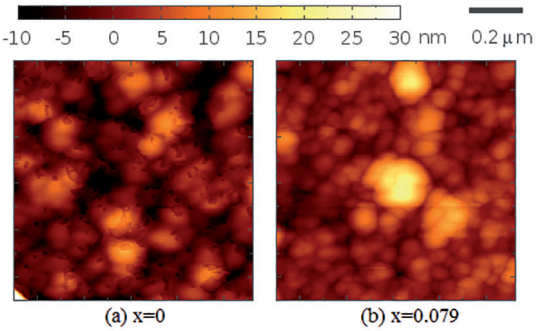

Figure 10: AFM surface images of $Cd_{1-x}Zn_xS$ films for (a) x = 0, and (b) x = 0.079

size for samples containing Zn. This result agrees with the trend observed for optical constants (see Figure 8), since a smaller particle size produces more particle boundaries and results in a reduction in refractive index. A reduction in particle size is expected if we consider growth through $M(OH)_2$ species (M = Zn or Cd), as mentioned previously. Therefore, this result is further evidence that a hydroxide growth mechanism becomes important when Zn is added to the reaction solution.

4. Conclusions

From a study of low Zn–$Cd_{1-x}Zn_xS$ thin films grown using a free-ammonia chemical bath method, it is possible to conclude that:

- The grown mechanism of the film is affected strongly by Zn concentration in solution bath; as Zn increases, the hydroxide growth mechanism becomes important, and decreases the deposition rate and crystallite size of the thin films.

- Independent of the Zn concentration in the solution bath, and hence Zn film content, a hexagonal structure was obtained in all analyzed cases; as expected, only a small decrease in lattice parameter resulted as Zn content increased.

- Optical measurements revealed samples with a high optical transmittance (up to 90%). The band gap values increase up to 2.6 eV as Zn content in the film increased. This high band gap obtained with low Zn content in the film (4.7 at.%) can be attributed to the presence of Zn and to quantum confinement effects since a decrease in crystallite size results from a change in grown mechanism.

It can be concluded that the main properties of the CdS window layer can be improved with small amounts of Zn in the film, which avoids an excessive mismatch with CIGS absorbent layer when in service, and improves device efficiency.

5. Acknowlegment

This work was supported by FONDECYT project N° 11090434, Grant CONICYT PFB-0824 and DIUC Project 210.011.050-1.0. C.A. Rodríguez appreciates the support provided by Conicyt through a Grant for Doctoral Thesis N° 21110556.

6. References

1. Kumar TP, Saravanakumar S, Sankaranarayanan K. Effect of annealing on the surface and band gap alignment of CdZnS thin films. *Applied Surface Science*. 2011;257(6):1923-1927.

2. Salem AM. Structure, refractive-index dispersion and the optical absorption edge of chemically deposited $Zn_xCd_{(1-x)}S$ thin films. *Applied Physics A*. 2002;74(2):205-211.

3. Hodes G. *Chemical Solution Deposition of Semiconductor Films*. New York: Marcel Dekker; 2002.

4. Clayton AJ, Irvine SJC, Jones EW, Kartopu G, Barrioz V, Brooks WSM. MOCVD of $Cd_{(1-x)}Zn_{(x)}S$/CdTe PV cells using an ultra-thin absorber layer. *Solar Energy Materials and Solar Cells*. 2012;101:68-72.

5. Devaney WE, Chen WS, Stewart JM, Mickelsen RA. Structure and properties of high efficiency ZnO/CdZnS/$CuInGaSe_2$ solar cells. *IEEE Transaction on Electron Devices*. 1990;37(2):428-433.

6. Chavhan SD, Senthilarasu S, Lee SH. Annealing effect on the structural and optical properties of a $Cd_{1-x}Zn_xS$ thin film for photovoltaic applications. *Applied Surface Science*. 2008;254(15):4539-4545.

7. Gaewdang N, Gaewdang T. Investigations on chemically deposited $Cd_{1-x}Zn_xS$ thin films with low Zn content. *Materials Letters*. 2005;59(28):3577-3584.

8. Carreón-Moncada I, González LA, Pech-Canul MI, Ramírez-Bon R. $Cd_{1-x}Zn_xS$ thin films with low Zn content obtained by an ammonia-free chemical bath deposition process. *Thin Solid Films*. 2013;548:270-274.

9. Burton LC, Hench TL. $Zn_xCd_{1-x}S$ films for use in heterojunction solar cells. *Applied Physics Letters*. 1976;29(9):612-614.

10. Reddy KTR, Reddy PJ. Studies of $Zn_xCd_{1-x}S$ films and $Zn_xCd_{1-x}S$/$CuGaSe_2$ heterojunction solar cells. *Journal of Physics D: Applied Physics*. 1992;25(9):1345-1348.

11. Khoshsirat N, Yunus NAM, Hamidon MN, Shafie S, Amin N. Analysis of absorber layer properties effect on CIGS solar cell performance using SCAPS. *Optik - International Journal for Light and Electron Optics*. 2015;126(7-8):681-686.

12. Rodríguez CA, Sandoval-Paz MG, Cabello G, Flores M, Fernández H, Carrasco C. Characterization of ZnS thin films synthesized through a non-toxic precursors chemical bath. *Materials Research Bulletin*. 2014;60:313-321.

13. Sandoval-Paz MG, Sotelo-Lerma M, Mendoza-Galvan A, Ramírez-Bon R. Optical properties and layer microstructure of CdS films obtained from an ammonia-free chemical bath deposition process. *Thin Solid Films*. 2007;515(7-8):3356-3362.

14. Sandoval-Paz MG, Ramírez-Bon R. Analysis of the early growth mechanisms during the chemical deposition of CdS thin films by spectroscopic ellipsometry. *Thin Solid Films*. 2009;517(24):6747-6752.

15. Tec-Yam S, Rojas J, Rejón V, Oliva AI. High quality antireflective ZnS thin films prepared by chemical bath deposition. *Materials Chemistry and Physics*. 2012;136(2-3):386-393.

16. Treumann WB, Ferris LM. The determination of a thermodynamic stability constant for the cadmium citrate ($CdCit^-$) complex ion at 25° by an E.M.F. method. *Journal of Americal Chemical Society*. 1958;80(19):5050-5052.

17. Martin RB. pH as a variable in free zinc ion concentration from zinc-containing lozenges. *Antimicrobial Agents Chemotherapy*. 1998;32(4):608-609.

18. Stipp SLS, Parks GA, Nordstrom DK, Leckie JO. Solubility-productconstant and thermodynamic properties for synthetic otavite, $CdCo_{3(s)}$, and aqueous associationconstnat for the Cd(II)-CO_2-H_2O system. *Geochimica et Cosmochimica Acta*. 1993;57(12):2699-2713.

19. Qian JW, Tao Y, Zhang WJ, He XH, Gao P, Li DP. Presence of Fe^{3+} and Zn^{2+} promoted biotransformation of Cd–citrate complex and removal of metals from solutions. *Journal of Hazardous Materials*. 2013;263(Part 2):367-373.

20. Roy P, Ota JR, Srivastava SK. Crystalline ZnS thin films by chemical bath deposition method and its characterization. *Thin Solid Films*. 2006;515(4):1912-1917.

21. Padam GK, Maholtra GL, Rao SUM. Studies on solution-grown thin films of $Zn_xCd_{1-x}S$. *Journal of Applied Physics*. 1988;63(3):770-774.

22. Azizi S, Dizaji HR, Ehsani MH. Structural and optical properties of $Cd_{1-x}Zn_xS$ (x = 0, 0.4, 0.8 and 1) thin films prepared using the precursor obtained from microwave irradiation processes. *Optik - International Journal for Light and Electron Optics*. 2016;127(18):7104-7114.

23. Hsiao CL, Palisaitis J, Junaid M, Persson POS, Jensen J, Zhao QX, et al. Room-temperature heteroepitaxy of single-phase $Al_{1-x}In_xN$ films with full composition range on isostructural wurtzite templates. *Thin Solid Films*. 2012;524:113-120.

24. Dridi Z, Bouhafs B, Ruterana P. First-principles investigation of lattice constants and bowing parameters in wurtzite $Al_xGa_{1-x}N$, $In_xGa_{1-x}N$ and $In_xAl_{1-x}N$ alloys. *Semiconductor Science and Technology*. 2003;18(9):850-856.

25. Cullity BD, Stock SR. *Elements of X-Ray Diffraction*. 3rd ed. London: Pearson; 2001.

26. Jana S, Maity R, Das S, Mitra MK, Chattopdhyay KK. Synthesis, structural and optical characterization of nanocrystalline ternary $Cd_{1-x}Zn_xS$ thin films by chemical process. *Physica E: Low-dimensional Systems and Nanostructures*. 2007;39(1):109-114.

27. Jacob KT, Raj S, Rannesh L. Vegard's law: a fundamental relation or an approximation? *International Journal of Materials Research*. 2007;98(9):776-779.

28. Murphy S, Chroneos A, Jiang C, Schwingenschlögl U, Grimes RW. Deviations from Vegard's law in ternary III-V alloys. *Physical Review B*. 2010;82(7):073201.

29. Zak AK, Majid WHA, Abrishami ME, Yousefi R. X-ray analysis of ZnO nanoparticles by Williamson–Hall and size–strain plot methods. *Solid State Sciences*. 2011;13(1):251-256.

30. Zawaideh E, inventor. Nondestructive Optical Techniques for Simultaneously Measuring Optical Constants and Thicknesses of Single and Multilayer Films.United States Patent US 5889592. 1999 Mar 30.

31. Pankove JI. *Optical processes in semiconductor*. Mineola: Dover Publications; 1976.

32. Cortés A, Gómez H, Marotti RE, Riveros G, Dalchiele EA. Grain size dependence of the bandgap in chemical bath deposited CdS thin films. *Solar Energy Materials and Solar Cells*. 2004;82(1-2):21-34.

33. Thangavel S, Ganesan S, Chandramohan S, Sudhagar P, Kang YS, Hong CH. Band gap engineering in PbS nanostructured thin films from near-infrared down to visible range by in situ Cd-doping. *Journal of Alloys and Compounds*. 2010;495(1):234-237.

34. Yoffe AD. Low-dimensional systems: Quantum size effects and electronic properties of semiconductor microcrystallites (zero-dimensional systems) and some quasi-two-dimensional systems. *Advances in Physics*. 2002;51(2):799-890.

35. Nanda KK, Sahu SN. One-Dimensional Quantum Confinement in Electrodeposited PbS Nanocrystalline Semiconductors. *Advanced Materials*. 2001;13(4):280-283.

36. Borse SV, Chavhan SD, Sharma R. Growth, structural and optical properties of $Cd_{1-x}Znx S$ alloy thin films grown by solution growth technique (SGT). *Journal of Alloys and Compounds*. 2007;436(1-2):407-414.

37. Raviprakash I, Bangera KV, Shivakumar GK. Preparation and characterization of $Cd_{1-x}Zn_xS$ thin films by spry pyrolysistechnique for photovoltaic applications. *Solar Energy*. 2009;83(9):1645-1651.

38. Verma U, Thakur V, Rajaram P, Shrivastara AK. Structural, morphological and optical properties of sprayed nanocrystalline thin films of $Cd_{1-x}Zn_xS$ solid solution. *Electronic Materials Letters*. 2015;11(1):46-54.